Interrelationships of Glycosylation and Aggregation Kinetics for *Peniophora lycii* Phytase†

Rasmus Høiberg-Nielsen,‡ Claus C. Fuglsang,§ Lise Arleth,|| and Peter Westh*,‡

Department of Life Sciences and Chemistry, Roskilde University, Building 18.1, P.O. Box 260, DK-4000 Roskilde, Denmark, Novozymes A/S, Krogshøjsvej 36, DK-2880 Bagsværd, Denmark, Danish Polymer Centre, Risoe National Laboratory, Frederiksborgvej 399, DK-4000 Roskilde, Denmark, and Department of Natural Sciences, The Royal Veterinary and Agricultural University, Thorvaldsensvej 40, DK-1871 Frederiksberg C, Denmark

Received November 9, 2005; Revised Manuscript Received March 3, 2006

ABSTRACT: The kinetics of thermally induced aggregation of the glycoprotein *Peniophora lycii* phytase (Phy) and a deglycosylated form (dgPhy) was studied by dynamic (DLS) and static (SLS) light scattering. This provided a detailed insight into the time course of the formation of small aggregates (∼10−100 molecules) of the enzyme. The thermodynamic stability of the two forms was also investigated using scanning calorimetry (DSC). It was found that the glycans strongly promoted kinetic stability (i.e., reduced the rate of irreversible denaturation) while leaving the equilibrium denaturation temperature, T_d, defined by DSC, largely unaltered. At pH 4.5−5.0, for example, dgPhy aggregated ∼200 times faster than Phy, even though the difference in T_d was only 1−3 °C. To elucidate the mechanism by which the glycans promote kinetic stability, we measured the effect of ionic strength and temperature on the aggregation rate. Also, the second virial coefficients (B_{22}) for the two forms were measured by SLS. These results showed that the aggregation rate of Phy scaled with the concentration of thermally denatured protein. This suggested first-order kinetics with respect to the concentration of the thermally denatured state. A similar but less pronounced correlation was found for dgPhy, and it was suggested that while the aggregation process for the deglycosylated form is dominated by denatured protein, it also involves a smaller contribution from associating molecules in the native state. The measurements of B_{22} revealed that dgPhy had slightly higher values than Phy. This suggests that dgPhy interacts more favorably with the buffer than Phy and hence rules out strong hydration of the glycans as the origin of their effect on the kinetic stability. On the basis of this and the effects of pH and ionic strength, we suggest that the inhibition of aggregation is more likely to depend on steric hindrance of the glycans in the aggregated form of the protein.

Glycosylation has a pronounced impact on protein stability in vivo as the glycan moieties prevent aggregation of newly synthesized proteins (see refs *1*−*3* for reviews). This effect is also seen in vitro where glycosylation of proteins leads to a higher kinetic stability (*4*−*6*). In addition, glycoproteins have a higher solubility than their nonglycosylated counterparts (*7*−*9*), and it therefore appears reasonable to conclude that glycosylation in general favors the dissolved monomeric form over adducts such as aggregates, precipitates, or crystals. While relationships between solubility and aggregation behavior of glycoproteins have been discussed in several reports (*10*−*12*), quantitative kinetic data on aggregation processes remain very sparse, and it follows that the mechanism underlying the effect of the glycans is poorly understood. One fundamental question is whether the glycans improve the interactions with the solvent or disrupt the packing in the precipitated form (or both), in other words, whether glycans act through the stabilization of the dissolved form or the destabilization of the precipitate.

Insight into how the glycans influence solubility and aggregation also appears to be important to biotechnology. Thus, for pharmaceutical and industrial applications, the physical instability of proteins is often a limiting parameter, particularly so in industrial applications where the conditions perturb the native conformation. However, aggregation may also hamper the utilization of enzymes under conditions where they are conformationally stable in a thermodynamic sense and at concentrations well below the solubility limit (*13*, *14*). This is particularly pertinent to storage stability. Therefore, for the greater part of biotechnology, the most important parameter is the kinetic stability and not the thermodynamic stability (*15*). In light of this, design of enzymes with new glycosylation sites appears to be of interest. However, rational use of glycosylation will require a much improved knowledge of how the glycans influence the surface properties of the protein.

The aim of this study is to elucidate how glycosylation influences an aggregation process far from equilibrium. As our model system, we have chosen the heavily glycosylated enzyme *Peniophora lycii* phytase (Phy)[1] and the enzymatically deglycosylated form of the enzyme (dgPhy). This

† This work was financially supported by Novo Nordisk Ltd. and Novozymes Ltd. through a scholarship to R.H.-N. We also acknowledge the support by the Carlsberg Foundation and The Danish Research Agency (Grants 26-02-0160 and 21-04-0087).

* To whom correspondence should be addressed. E-mail: pwesth@ruc.dk. Telephone: +45 46742879. Fax: +45 46743011.

‡ Roskilde University.

§ Novozymes A/S.

|| Risoe National Laboratory and The Royal Veterinary and Agricultural University.

10.1021/bi0522955 CCC: $33.50
Published on Web 03/24/2006

system is particularly suited for the purpose since earlier work has shown that deglycosylation has practically no influence on the enzymatic activity (*16*). On this basis, it was concluded that the peptide structure retains the native fold following removal of the glycans and hence that comparisons of the properties of Phy and dgPhy indeed highlight the direct effects of the saccharides. We have employed static light scattering (SLS) and dynamic light scattering (DLS) which readily detects the time course of the aggregation process from the earliest events, where the average cluster size is only a few protein molecules. To gain insight into the hydration of the two glycoforms, we also measured second virial coefficients by SLS.

MATERIALS AND METHODS

Purification. The heavily glycosylated enzyme *P. lycii* phytase (molecular mass of ~65 kDa) possesses 10 N-glycosylation sites containing heterogeneous glycans, which constitute more than 20% of the total mass. It is systematically named *myo*-inositol hexakisphosphate phosphohydrolase (EC 3.1.3.26), which reflects its catalytic function and initial position preference, as it catalyzes the release of inorganic phosphate from *myo*-inositol hexakisphosphate (*17*). *P. lycii* phytase was obtained from a batch of Bio-Feed Phytase (Novozymes, Bagsværd, Denmark) produced in *Aspergillus oryzae* and was purified as previously described (*18*). A change of order was made to the procedure, as the filtered broth was first applied to a Phenyl Sepharose column (Amersham Pharmacia Biotech, Piscataway, NJ) before it was applied to a Q-Sepharose FF column (Amersham Pharmacia Biotech). The phytase eluate was dialyzed extensively against 20 mM sodium acetate (pH 5.5) in a Spectra/Pore (Spectrum Laboratories, Inc., Rancho Dominguez, CA) membrane (12−14 kDa cutoff) to a final conductivity of 1 mS/cm. The dialyzed solution was concentrated on a Millipore Amicon cell (Millipore, Billerica, MA) with a cutoff of 10 kDa to a final concentration of 90.6 mg/mL ($\epsilon = 1.0\ M^{-1}\ cm^{-1}$) with a purity of 1.90 (280 nm/260 nm). SDS−PAGE (5 μg/well) showed only one band with a molecular mass of ~65 kDa, because of which it is assumed that the purity was higher than 95%.

SDS−PAGE and Isoelectric Focusing. SDS−PAGE was carried out on tris-glycine−polyacrylamide gels with a gradient of 8 to 16% tris-glycine (Invitrogen, Carlsbad, CA), and isoelectric focusing was performed with Ampholine PAGplate (pH 3.5−9.0) (Amersham Biosciences, Buckinghamshire, U.K.). All gels were washed three times in demineralized water and stained for 60 min with GelCode Blue stain reagent (Pierce Biotechnology, Inc., Rockford, IL). Subsequently, the gels were washed for 60 min with demineralized water and scanned digitally. pI values were determined by isoelectric focusing to be 3.62 and 3.58 ± 0.05 for Phy and dgPhy, respectively (manufacturer's uncertainty).

Measurements of Enzyme Activity. The enzymatic activity was measured by diluting samples in 0.1 M sodium acetate with 0.01% (w/v) Tween 20 (pH 5.5). The enzyme samples were further diluted 26 times as a 10 μL enzyme dilution was transferred to 250 μL of 37 °C preheated substrate [5 mM sodium phytate (Sigma catalog no. P-8810), 0.1 M sodium acetate, and 0.01% Tween 20 (pH 5.5)]. After the samples were incubated at 37 °C for 30 min, an equal volume of 10% (w/v) trichloroacetic acid was added to terminate the reaction. The concentration of free inorganic phosphate was measured by adding an equal amount of molybdate reagent [100 mL of molybdate reagent contains 7.32 g of $FeSO_4 \cdot 7H_2O$, 1.0 g of $(NH_4)_6Mo_7O_{24} \cdot 4H_2O$, and 3.2 mL of H_2SO_4]. Absorbance was measured on a microplate reader (Molecular Devices, Sunnyvale, CA) at 750 nm, and the phosphate concentration was calculated by making an appropriate standard graph (0.25−2 mM KH_2PO_4). The specific enzymatic activity was calculated as the turnover rate, specified as the amount of enzyme that catalyzes the release of 1 μmol of phosphate/min. The activity was calculated with the equation activity = $(26PK)/(30C)$ μmol of PO_4^{3-} mL^{-1} min^{-1}, where P is the concentration of PO_4^{3-}, K is the dilution factor, and C is the enzyme concentration. We found specific activities of both phytase and the deglycosylated variant in the range of 1300−1500 units/mg. This is comparable to the value reported by Lassen et al. (*18*) (~1100 units/mg). More importantly, we did not find any reduction in activity following deglycosylation. For a compact globular protein like phytase, this strongly suggests that the overall fold of the peptide remains unchanged. This conclusion has been further substantiated by synchronous radiation circular dichroism, which showed practically identical spectra for the two glycoforms (H. L. Bagger, personal communication).

Deglycosylation. Enzymatic deglycosylation of phytase was carried out with the endoglycosidase endo-β-*N*-acetylglycosaminidase F_1 (EC 2.2.1.96) better known as Endo F_1 (molecular mass of 32 kDa). The enzyme releases the glycans by hydrolyzing the glycosidic bond between the two *N*-acetylglucosamine groups that connect the polysaccharide with the protein, so the deglycosylated enzyme has one *N*-acetylglucosamine group attached on each of the 10 glycosylation sites (*19*).

The following reaction mixture was used: 11 mL of phytase solution (90.6 mg/mL), 4.5 mL of Endo F_1 (0.093 mg/mL, Novozymes), and 15 mL of reaction buffer [50 mM sodium citrate and 20 mM EDTA-NaOH (pH 6.0)]. The reaction mixture was allowed to react for 48 h at 37 °C. Subsequently, the reaction product exhibited only one band on a SDS−tris-glycine gel (5 μg/well) with maximal intensity around 47−48 kDa. Prolonged treatment with Endo F_1 did not reduce the molecular mass of the deglycosylated product further (H. L. Bagger, personal communication). While some polydispersity must be expected, this observation and the weight loss derived from SDS−PAGE suggest that dgPhy used in this study is dominated by the form with one *N*-acetylglucosamine on each site, i.e., the maximal degree

[1] Abbreviations: B_{22}, second virial coefficient; C, protein mass concentration; C_p^E, excess heat capacity function; D, denatured protein; d*n*/d*C*, refractive index increment; dgPhy, deglycosylated *P. lycii* phytase; DLS, dynamic light scattering; DSC, differential scanning calorimetry; endo F_1, endo-β-*N*-acetylglycosaminidase F_1; $I_{initial}$, initial average light scattering; I_0, intensity of the laser; $I_{background}$, background scattering; I_t, average light scattering; K, light scattering optical constant; M, molecular weight of the scattering particles; MW, molecular weight; N, native protein; N_A, Avogadro's number; n_0, refraction index of the solvent; NS, normalized size; Phy, *P. lycii* phytase; R_θ, Rayleigh ratio; SLS, static light scattering; SDS−PAGE, sodium dodecyl sulfate−polyacrylamide gel electrophoresis; T_d, denaturation temperature; $\chi_d(T)$, fraction of denatured protein; $\chi_n(T)$, fraction of native protein; λ_0, wavelength of the laser beam in a vacuum.

of deglycosylation expected for this endoglycosidase. The reaction mixture was dialyzed twice for 24 h using Spectra/pore (Spectrum Laboratories) dialysis membranes (12−14 kDa cutoff) in 5 L of dialysis buffer [50 mM sodium acetate (pH 5.5)]. The dialyzed solution contained both Endo F_1 and deglycosylated phytase in a molar ratio of ∼1:1000.

Sample Preparation. The same buffer solutions were used for calorimetry and light scattering experiments: 50 mM sodium acetate at pH 4.5−5.5 and 50 mM HEPES at pH 6.5−8.5. Stock solutions were diluted in the appropriate buffer solution in 3 mL vials and kept on ice. pH measurements were performed on all samples with a model 420 A Orion pH-meter (Thermo Electron Corp., Philadelphia, PA). When necessary, the pH was adjusted with HCl/NaOH.

Calorimetry. The thermal stability of Phy and dgPhy was determined by differential scanning calorimetry (DSC). The calorimeter was a MicroCal MC-2 scanning calorimeter (MicroCal, Northampton, MA) with a cell volume of 1.2 mL. The protein concentration was 3.0 mg/mL, and the scans covered the 30−90 °C interval at a rate of 45 °C/h. First, the dependence on pH of the denaturation temperature, T_d, defined as the maximum of the DSC trace was determined. Second, the data were used to assess the fraction of unfolded protein molecules as a function of temperature, $\chi_d(T)$. For a given temperature, T', this fraction may be approximated as the ratio of the peak area up to T' and the total area of the transition peak (this approach neglects the temperature dependence of the denaturation enthalpy in the ∼10 °C temperature interval of the DSC peak). Thus, $\chi_d(T)$ may be written as a function of the excess heat capacity function (C_p^E) recorded by the calorimeter

$$\chi_d(T) = \int_{-\infty}^{T'} C_p^E \, dT / \int_{-\infty}^{\infty} C_p^E \, dT \quad (1)$$

The fraction of native protein [$\chi_n(T)$] can be determined

$$\chi_n(T) = 1 - \chi_d(T) \quad (2)$$

Light Scattering Measurements. The light scattering experiments were performed on a combined SLS-DLS instrument (Brookhaven Instruments, Holtsville, NY). It consists of a BI-200SM goniometer with a 632.8 nm HeNe laser with a power of 35 mW. A BI-APD Avalanche photodiode detector detects the signal, which is subsequently treated in a BI-9000AT digital autocorrelator (522 channels). Temperature is controlled within ±0.1 °C by a water bath. Prior to the measurements, the samples were kept on ice and filtered three times through 0.22 μm disposable filters. Circular glass tubes (12 mm) were used as sample cells. Before being used, they were rinsed in ethanol and MilliQ water and air-dried. Except for the measurements of second virial coefficients (see below), the protein concentration was 1 mg/mL in all light scattering experiments.

Measurements of Virial Coefficients by SLS. SLS was used to measure second virial coefficients (B_{22}), and data were analyzed according to the Zimm equation (*20*):

$$\frac{KC}{R_\theta} = \frac{1}{M} + 2B_{22}C \quad (3)$$

where R_θ represents the Rayleigh ratio at the angle θ, C is the protein mass concentration, and M is the molecular weight of the scattering particles. K is the light scattering optical constant related to the polarizability of the particles:

$$K = \frac{4\pi^2 n_0^2 (dn/dC)^2}{N_A \lambda_0^4} \quad (4)$$

Where n_0 is the refraction index of the solvent, λ_0 is the wavelength of the laser beam in a vacuum, N_A is Avogadro's number, and dn/dC is the refractive index increment. For most proteins in solution, dn/dC is ∼0.18−0.20 mL/g. In this work, 0.185 was used as the dn/dC value. The measurements were performed at 20 °C with 10−12 concentrations from 0.5 to 5 mg/mL. The Rayleigh constant was measured at four detector angles (45°, 60°, 90°, and 120°), and toluene was used as the calibration liquid.

Measurements of Aggregation Kinetics. The aggregation was followed by means of SLS and DLS. SLS intensity was used as an indicator for the aggregation process, whereas DLS was primarily used to ensure that the samples were not preaggregated at the beginning of the experiment. The two types of measurements were performed, simultaneously, at a detector angle of 90°.

The obtained autocorrelation functions were analyzed with software provided by Brookhaven Instruments (9KDSLW) using the second-order cumulant method. Simultaneously, the time average intensity of the light scattering was used to indicate the events of aggregation, by subtracting the background scattering ($I_{background}$) from the average intensity of light scattered by the sample (I_t) and dividing by the average intensity at the beginning of the aggregation process ($I_{initial}$):

$$\text{normalized size} = (I_t - I_{background})/(I_{initial} - I_{background}) \quad (5)$$

Equation 5 states how many times the average molecular mass of the dissolved particles has increased as a function of time, and it will be termed the normalized size (NS). The validity of this equation is evident from the relationship between the Rayleigh ratio (R_θ) and the molecular weight of the dissolved particles (M):

$$R_\theta = \frac{i_\theta}{I_0} \frac{r^2}{1 + \cos^2\theta} = KCM \quad (6)$$

where i_θ is the scattering intensity at the angle θ, I_0 is the intensity of the laser, and r is the distance between the detector and the scattering molecules. Because all other quantities are constant, i_θ is directly proportional to M. The relation is only valid as long as the conditions of Rayleigh scattering are maintained (*21*), i.e., as long as $D \ll \lambda$. As a rule of the thumb, we used $D = 1/(20\lambda) \approx 32$ nm, corresponding to an NS of ∼350.

RESULTS

Differential Scanning Calorimetry (DSC). Representative results from the DSC measurements are illustrated in Figure 1. The denaturation temperature (T_d), defined as the maximum of the peak, was measured at several pH values, and the results are listed in Table 1.

It appears (Table 1) that T_d depends only weakly on the glycosylation. In general, the denaturation occurs a few

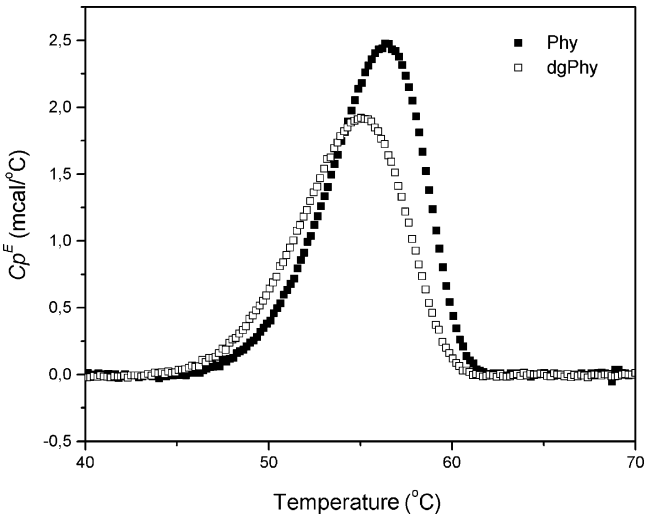

FIGURE 1: DSC data showing the thermal denaturation of Phy (■) and dgPhy (□) at pH 5.0.

Table 1: Transition Temperature (T_d) of Phy and dgPhy for pH 4.5−8.5[a]

pH	T_d of Phy (°C)	T_d of dgPhy (°C)	pH	T_d of Phy (°C)	T_d of dgPhy (°C)
4.50	59.1	56.4	6.50	56.8	53.9
5.00	56.6	55.4	7.50	43.7	39.3
5.25	57.3	56.5	8.50	27.9	24.1
5.50	57.4	58.3			

[a] The reproducibility of T_m is better than 0.5 °C.

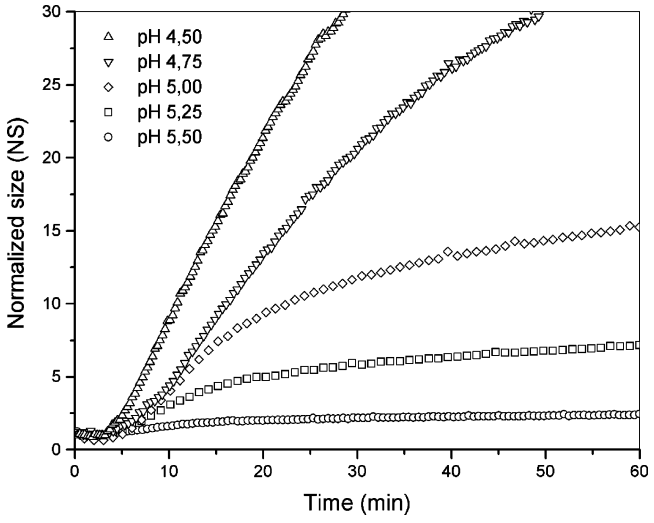

FIGURE 2: Time course of aggregation of Phy at T_d (see Table 1) as a function of pH.

degrees higher for Phy than for dgPhy, but at pH 5.50, the deglycosylated variant is marginally more thermostable.

Thermally Induced Aggregation as a Function of pH. Heat-induced aggregation at T_d (see Table 1) was examined at five pH values between 4.5 and 5.5 with static light scattering (SLS). This pH range was chosen because Phy is prone to reversible precipitation at pH <4.5, while it shows limited aggregation at pH >5.5. The measurements showed that the rate of aggregation for dgPhy was noticeably higher than the rate for Phy (Figures 2 and 3), particularly so in the lower end of this pH interval. At pH 5.0, for example, the average aggregates of Phy grow to include four protein molecules

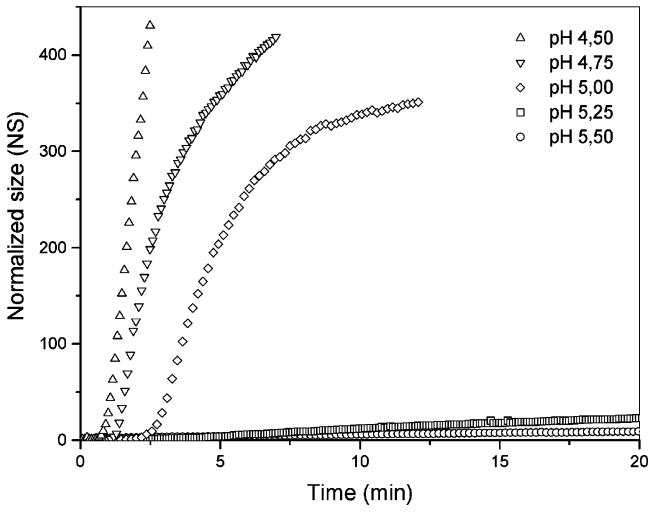

FIGURE 3: Time course of aggregation of dgPhy at T_d as a function of pH. The figure highlights the pronounced increase in the aggregation rate when the pH is lowered, particularly between pH 5.25 and 5.00.

Table 2: Aggregation Kinetics of Phy and dgPhy as a Function of pH[a]

pH	Phy (NS/min)	dgPhy (NS/min)	pH	Phy (NS/min)	dgPhy (NS/min)
5.50	0.12	0.4	4.75	0.89	165
5.25	0.28	1.4	4.50	1.24	299
5.00	0.66	90			

[a] The deglycosylated variant consistently aggregates at a higher rate, and the increase in rate over the investigated pH interval is almost 2 orders of magnitude higher for dgPhy than for Phy.

in 10 min (Figure 2). For dgPhy, on the other hand, the average aggregate accumulates ~350 protein molecules over the same period (Figure 3). To enable more direct quantitative comparisons of the aggregation kinetics, we empirically partitioned these curves into three phases, which are commonly found in the data for both glyco forms. The first is a lag phase in which no growth in NS can be detected (1). The lag is assumed to reflect thermal equilibration after the sample is placed in the instrument and the nucleation behavior of the aggregation process. The second is a phase of near-linear relationship of NS and time (2). The third is a phase with negative curvature reflecting a gradual reduction in aggregation rate (3). It should be noted that features other than these specified three can be detected. For example, a strong (exponential) growth in NS occurs between features 1 and 2. Also, not all of these phases can be detected in all trials. Phase 3, for example, is generally absent at the higher pH values.

In the following, we will use the slope in phase 2 to compare the aggregation kinetics. Linear fits to phase 2 in Figures 2 and 3 give the rates listed in Table 2. The unit is NS min^{-1}, corresponding to the average number of protein molecules that each cluster adsorbs per minute.

Table 2 shows that dgPhy had the fastest aggregation rate at all pH values. At pH 5.5, the aggregation rate of dgPhy was 3 times faster than the rate of Phy; however, this difference increased as the pH was lowered, and at pH 4.5, the difference was more than a factor of 240.

Aggregation Rate as a Function of Ionic Strength. The influence of ionic strength on the aggregation process was

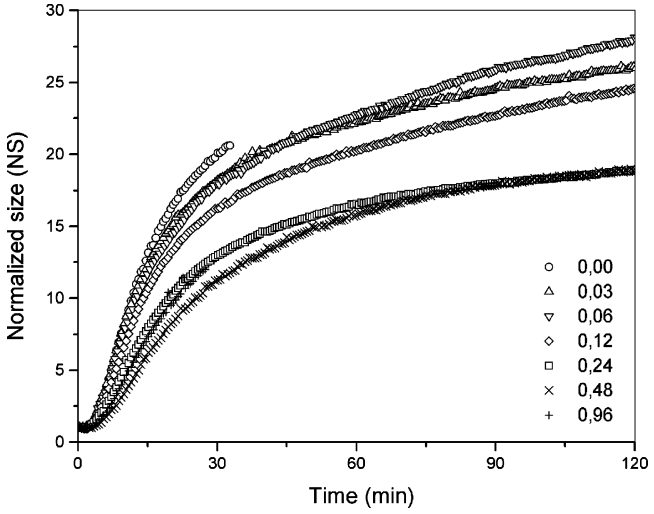

FIGURE 4: Raw SLS data for aggregation of Phy as a function of ionic strength. The numbers at the symbols are the ionic strengths in molar units.

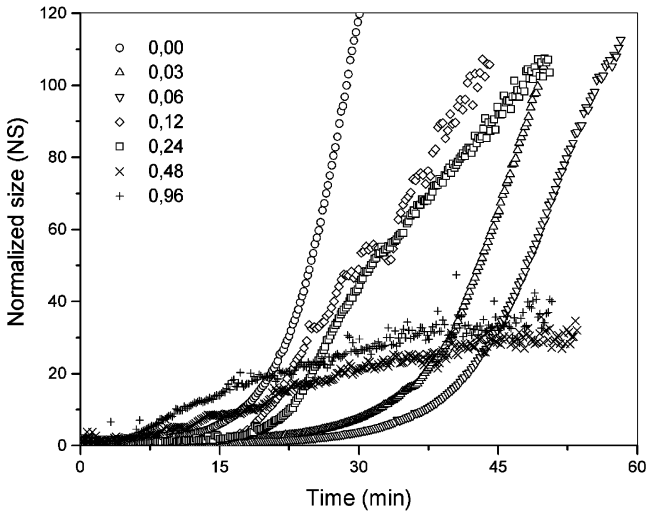

FIGURE 5: Aggregation of dgPhy as a function of ionic strength (molar units).

investigated with SLS at seven NaCl concentrations covering the 0−0.96 M range and at pH 5.0. Pronounced differences in the rate of aggregation may influence the dynamics of the ion−protein interactions, and we consequently chose experimental temperatures (57.4 °C for Phy and 40 °C for dgPhy) which generated comparable aggregation rates for the two forms. The time courses of the aggregation process are plotted in Figures 4 and 5.

Increasing ionic strength slowed the aggregation rate, but the salt affected the NS function differently for the two glycoforms. Thus, for Phy, the salt gradually delayed aggregation without changing the overall course of NS (Figure 4). For dgPhy, on the other hand, NaCl changed the initial part of the NS function from convex to concave. Moreover, the lag period, phase 1, was reduced by the salt for dgPhy (Figure 5) but was unaffected for Phy (Figure 4). The effect of NaCl is further illustrated in Figures 6 and 7, which show the aggregation rate (defined in the same way as in Table 3) as a function of the salt concentration.

It appears that the aggregation rate of Phy is reduced by a factor of 2 when the concentration of NaCl is increased

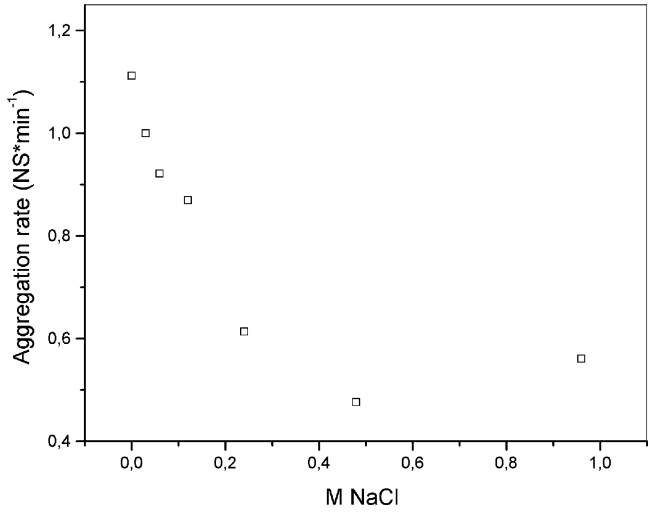

FIGURE 6: Aggregation rate of Phy as a function the molar concentration of NaCl.

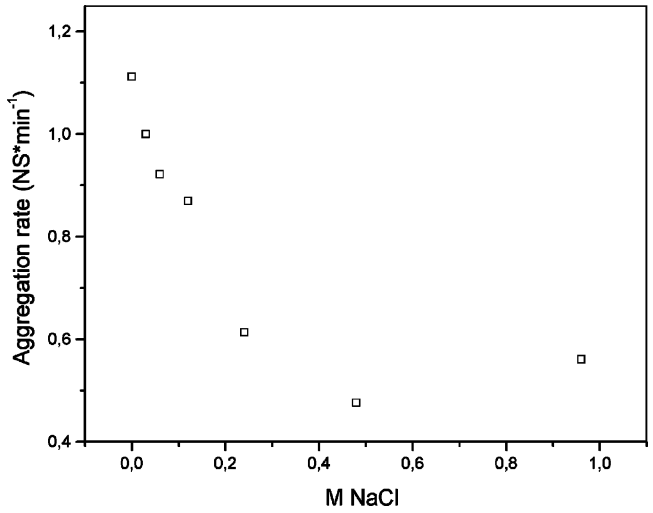

FIGURE 7: Aggregation rate of dgPhy as a function the molar concentration of NaCl.

Table 3: Second Virial Coefficients, B_{22} (±standard error of the mean) of Phy and dgPhy Measured at 20 °C

	B_{22} ($\times 10^4$ mL mol g^{-2})	
pH	Phy	dgPhy
6.50	7.10 ± 1.40	7.90 ± 1.80
5.50	4.71 ± 0.16	5.25 ± 0.24
5.25	3.10 ± 2.40	4.90 ± 2.80

from 0 to 0.5 M. The effect on dgPhy is more pronounced, as the aggregation rate decreases by a factor of 10 in the same concentration range.

Effect of Temperature. The aggregation of Phy and dgPhy was investigated as a function of temperature at pH 5.0. The experimental temperatures were chosen to cover the interval of the denaturation peak in the DSC trials (cf. Figure 1), and representative SLS results are shown in Figures 8 and 9.

As expected, the aggregation rate increased with temperature. The rate for dgPhy was very high at temperatures above the T_d, and the scattering intensity had to be averaged over short time intervals. This made the data more noisy than the corresponding Phy data (cf. Figures 8 and 9).

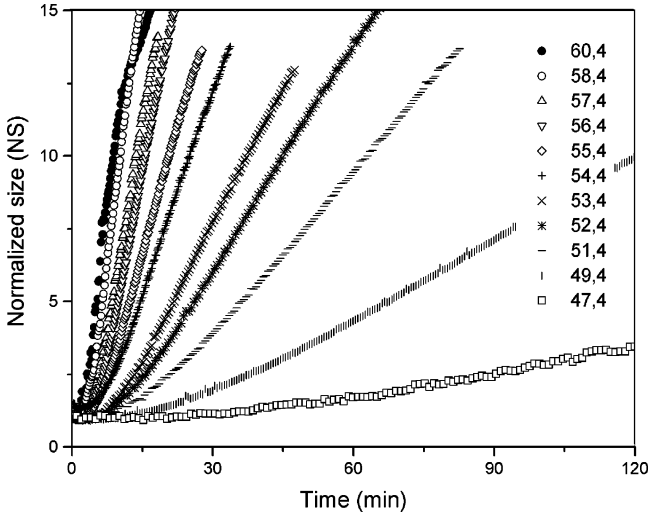

FIGURE 8: Time course of the aggregation of Phy at pH 5.0 as a function of temperature (degrees Celsius).

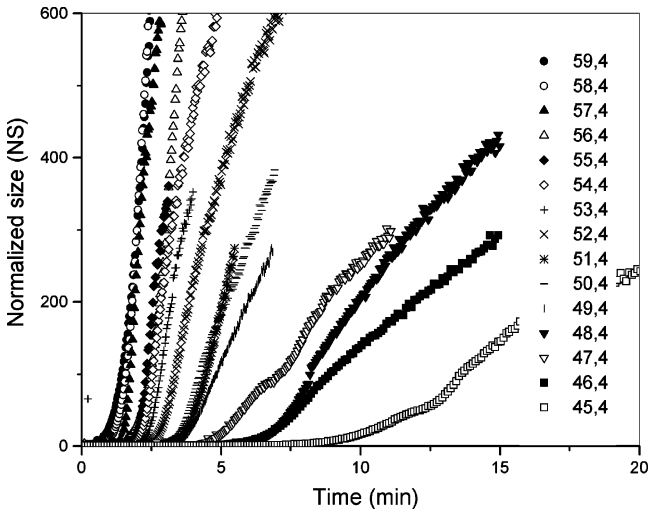

FIGURE 9: Time course of the aggregation of dgPhy at pH 5.0 as a function of temperature (degrees Celsius).

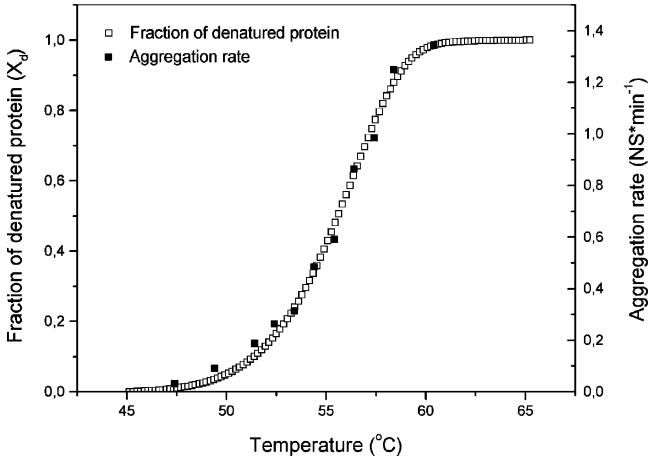

FIGURE 10: Aggregation rate of Phy (right-hand ordinate, ■) and fraction of denatured protein, $\chi_d(T)$ (left-hand ordinate, □), as a function of temperature at pH 5.0.

The temperature dependence of the aggregation rates is illustrated in Figures 10 and 11 together with the extent of the denaturation process, $\chi_d(T)$ (eq 1).

It appears from Figure 10 that the aggregation rate is practically proportional to the $\chi_d(T)$ function throughout the

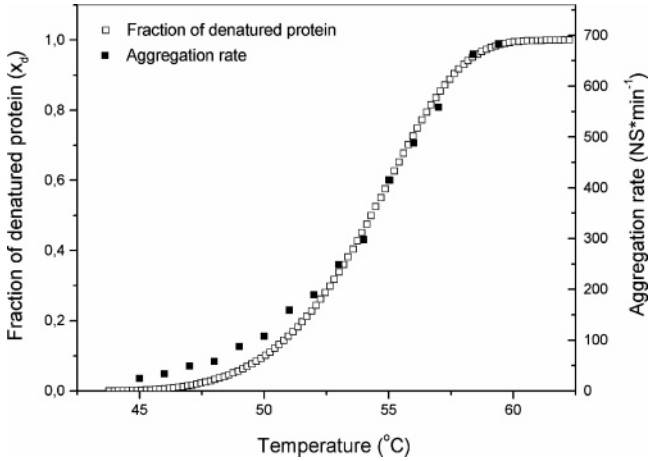

FIGURE 11: Aggregation rate of dgPhy (right-hand ordinate, ■) and fraction of denatured protein, $\chi_d(T)$ (left-hand ordinate, □), as a function of temperature at pH 5.0.

investigated temperature interval (the two functions can be scaled to superimpose). This strongly suggests that the rate of the aggregation process is governed by the concentration of thermally denatured protein, [D] (see Discussion). For dgPhy, this correlation is somewhat less pronounced (Figure 11). Attempts to find a common scaling factor for the two functions through nonlinear, least-squares fitting of a sigmoidal function suggested a systematic, positive deviation of the aggregation rate for temperatures below ~52 °C (Figure 11). The aggregation rate at the lowest temperatures in Figure 11, where the population of thermally denatured protein [$\chi_d(T)$] approaches zero, is ~4% of the rate when all protein is unfolded [$\chi_d(T) = 1$].

Virial Coefficients. Second virial coefficients (B_{22}) of Phy and dgPhy were measured by SLS. Results for measurements at pH 5.25−6.50 are listed in Table 3. At lower pHs, association of native protein precluded measurements of B_{22}.

It appears that B_{22} is positive for both of the forms (Table 3) and that it increases with pH. More importantly, B_{22} is consistently higher for dgPhy than for Phy.

DISCUSSION

Aggregation Mechanism. Protein aggregation is a complex phenomenon compared to crystallization. This is due to the fact that it is not the native form, but an unfolded or partially unfolded form, of the protein that associates (*22*−*25*). Therefore, the process may be more related to protein folding than to processes involving association of molecules in the native conformation (*26*). In a simplified molecular picture, heat-induced aggregation may be explained as a two-step reaction, where the first step involves the breakdown of the native conformation (the denatured structure may, however, retain several structural elements reminiscent of the native protein). This equilibrium process is followed by an irreversible (i.e., far from equilibrium) aggregation of the denatured protein. As originally suggested by Lumry and Eyring (*27*) and later applied to the description of protein aggregation by other workers (*28*−*30*), this can expressed

$$\mathrm{N} \leftrightarrow \mathrm{D} \rightarrow \mathrm{A} \qquad (7)$$

where N, D, and A represent native, denatured (monomeric), and aggregated protein, respectively. Earlier work with Phy

and dgPhy (*16*) suggested that short exposures to temperatures around T_d indeed induced a reversible thermal denaturation of the protein. This supports the molecular picture for aggregation illustrated in eq 7, and several aspects of this work may be analyzed with respect to this approach. For example, the rates listed in Table 2 are comparable in the sense that the concentration of the "substrate" or reactant for the aggregation, D, is similar for all data. This follows from the choice of working at the temperature T_d, where (close to) 50% of the protein molecules are in the D state ($\chi_d \cong 0.5$). More importantly, eq 7 may be used to rationalize the relationship between the temperature dependence of the aggregation rate and χ_d (i.e., the initial concentration of the D form) illustrated in Figures 10 and 11. The fact that these two functions are practically proportional for Phy (Figure 10) supports the view (eq 7) that aggregation predominantly involves association of a denatured form and further suggests that the process follows first-order kinetics. We note that since we use the experimental temperature to vary the concentration of D, the effects of concentration and temperature cannot be assessed independently. Because of the rather invariant T_d (Table 1), however, the temperature changes only a few degrees for the data in Table 2. Another condition for this interpretation is that pronounced precipitation around T_m is absent in the DSC trials. Thus, an exothermic aggregation would tend to skew the $\chi_d(T)$ function toward the left at the higher temperatures in Figures 10 and 11. The stable post-transition baseline (Figure 1 and ref *16*) supports the assumption of limited aggregation in the DSC trials (cf. ref *31*). First-order kinetics have previously been found in a number of works on heat-induced aggregation of proteins (*32*−*36*) and may reflect a process governed by the addition monomeric denatured proteins to a pre-established aggregate (*37*, *38*), although other reaction schemes cannot be ruled out on the basis of the current data.

For dgPhy (Figure 11), the correlation of the initial concentration of the D form (χ_d) and the rate of aggregation was largely similar to that of Phy discussed above. However, the two curves could not be superimposed over the entire temperature interval. Attempts to find the best scaling factor through nonlinear regression suggested that while the aggregation of dgPhy predominantly proceeds via the D form there is an additional aggregation involving direct association of N forms. This "leak flux" appears to have a rate of ∼4% of the rate of aggregation of denatured dgPhy. Although this aggregation of N forms is rather limited in the temperature interval investigated here, it may well become very important at lower temperatures where χ_d is practically zero, and the flow described by eq 7 may thus be eliminated. For example, the in vitro lifetime of the active protein might depend critically on this irreversible native aggregation.

The conclusions about the temperature dependence described above also provide access to the estimation of an apparent activation energy, E_a, for the second reaction in eq 7. Thus, the rate constant for this (first-order) process is proportional to $NS/\chi_d(T)$ [since $\chi_d(T)$ is proportional to the concentration of D]. Plots of $\ln[NS/\chi_d(T)]$ versus $1/T$ (not shown) indicated Arrhenius activation energies of 60 and 10 kJ/mol for Phy and dgPhy, respectively. These values are rather small compared to earlier reports on soluble proteins for which E_a has typically fallen in the 50−400 kJ/mol range (*39*−*43*).

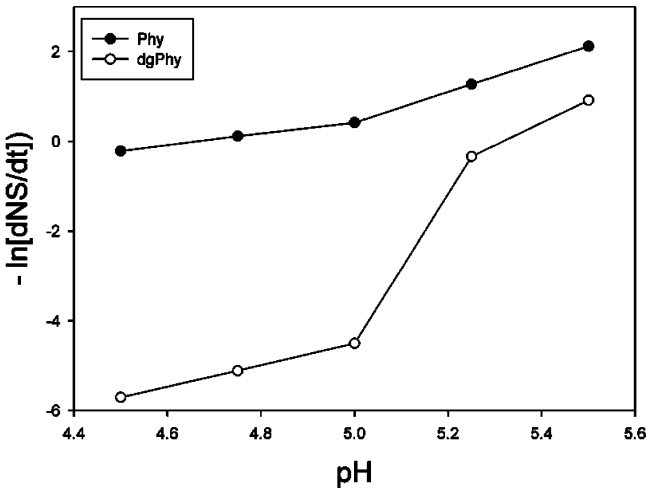

FIGURE 12: Negative value of the logarithm of the aggregation rate, $-\ln(dNS/dt)$ as a function of pH.

Effect of pH and Ionic Strength. To discuss effects of pH and ionic strength, we tentatively partition the interactions involved in the aggregation process into two categories: (i) repulsive Coulombic forces which arise from the (equal) average charge of the protein molecules (this effect will increase with aggregate size) and (ii) other interactions including Coulombic and hydrophobic forces, which may either favor or hamper aggregation and which are independent of aggregate size.

The data in Table 2 show that the rate of aggregation decreases strongly as the pH is increased from 4.5 to 5.5. Since the isoelectric point of both forms was 3.6, this behavior most likely reflects the electrostatic repulsion, (i) which becomes stronger as the pH moves away from the pI. The observation of equal pI suggests that the strength of category (i) will be similar for the two forms at a given pH. Still, rather different pH effects are observed. This is illustrated in Figure 12 which shows the negative logarithm of the aggregation rate, $-\ln(dNS/dt)$, as a function of pH. The rationale for this plot relies on the first-order kinetics suggested above and the fact that [D] is constant [$\chi_d(T) \approx 0.5$] for all data in Table 2. If the small differences in temperature are neglected, it follows that the measured aggregation rates (Table 2) are proportional to the rate constant ($k \approx 1/[D] \times dNS/dt$ at all pH values). Hence, according to the Arrhenius equation ($-\ln k = E_a/RT - \ln A$), the ordinate in Figure 12 scales linearly with the activation energy, E_a, of the irreversible reaction in eq 7.

The figure indicates an anomaly in the activation energy around pH 5.0 for both glyco forms. For Phy, the curve bends upward at this pH, while for dgPhy, it shows a steep increase. This behavior suggests that one (or more) critical amino acid is titrated at this pH [while the shallow positive slope of both curves at lower pH probably reflects the pH dependence of the (i) repulsion]. The much greater increase in E_a for dgPhy could be due to a shielding effect by the glycans. Thus, if lowering the pH beyond 5.0 permits a specific ion−ion interaction, which strongly promotes aggregation, sterical hindrance of close approach by the oligosaccharides in Phy could offset the impact of this titration.

These observations point toward favorable, specific (i.e., structurally well defined) electrostatic interactions in the aggregate, and this is further illustrated by the effect of the

ionic strength (Figures 6 and 7). Thus, the increase in ionic strength up to ~0.5 M strongly reduces the aggregation rate for both glyco forms. It also shows that despite the repulsion discussed for category (i), the net effect of electrostatic interactions on the aggregation rate is favorable. This emphasizes the importance of specific ion−ion contacts in the aggregate, and the fact that the slope in Figure 7 (dgPhy) is almost 1 order of magnitude larger than the slope in Figure 6 (Phy) again hints that the glycans may weaken the electrostatic interactions through steric hindrance. The interpretation of the ionic strength data is limited by the fact that χ_d and T cannot be varied independently in these experiments. Hence, the results illustrated in Figures 4−7 may rely in part on a salt effect on the equilibrium step in eq 7. It is noteworthy, however, that NaCl is close to the center of the so-called Hofmeister series and thus in general exerts a limited displacement on N ↔ D equilibria (*44*, *45*).

Finally, an interesting qualitative aspect of the pH dependence appears from Figures 2 and 3, in which the curves flatten off (i.e., enter phase 3) earlier as the pH is lowered. This means that the decrease in aggregation rate occurs earlier for systems with lower rates of aggregation. In fact, the most rapidly aggregating system (dgPhy at pH 4.5) shows no sign of phase 3 even as the normalized aggregate size reaches 400. This is probably also a consequence of the pH-dependent changes in the electrostatic repulsion (*46*). If, on the other hand, the aggregation was diffusion-limited, e.g., as a result of a local depletion of monomers, the reverse correlation between the aggregation rate and the entry into phase 3 would be observed. This latter type of behavior is commonly found for crystallization processes (*47*).

Hydration and the Second Virial Coefficient. The second virial coefficient, B_{22}, quantifies the thermodynamic nonideality of the solution. Positive values, as we find here (Table 3), reflect either favorable water−protein interaction (strong hydration) or repulsive protein−protein interactions. The latter is dominated by the electrostatic repulsion, and the minimal value of B_{22} hence generally occurs when pH = pI (*48*). This behavior is also reflected in the pH dependence observed here (Table 3) since B_{22} increases with pH (pH > pI throughout Table 3) for both variants. Interestingly, B_{22} is larger for (native) dgPhy than for (native) Phy. Since deglycosylaion had no detectable effect on pI, the mutual electrostatic repulsion for the two variants is likely to be similar, and the difference in B_{22} may reflect more favorable hydration of dgPhy and/or enhanced repulsion due to the glycan moieties of Phy. Previous investigations of the Phy/dgPhy system have suggested that peptide−water interactions are indeed more favorable than glycan−water interactions (*16*, *49*). Thus, a favorable hydration of the glycans in Phy (and a concomitant stabilization of the dissolved, monomeric D state) can most likely be ruled out as a mechanism underlying the slower aggregation of the glycoprotein. Rather and in accord with the previous discussion, the data in Table 3 point toward disruption of attractive forces in the growing aggregate as the reason for the slower aggregation of the Phy.

These results (Table 3) may also be pertinent to discussions of relationships between glycosylation and the (equilibrium) solubility of proteins. Glycans have been shown to affect the solubility substantially (*7*−*12*), but only few systematic studies (*50*, *51*) have been carried out. It has been argued that the increased solubility generally found for the glycosylated forms depends on the solubility properties of the carbohydrates (*51*). If, however, water interacts more favorably with the peptide than the glycan moiety, favorable water−glycan interactions cannot be important for the high solubility of phytase. It appears that establishing if this is a general trend for glycoproteins is of interest.

Conclusion. Deglycosylation has a limited effect on the equilibrium heat denaturation of phytase (Table 1). In accordance with data for other glycoproteins (*52*−*57*), T_d is shifted only a few degrees upon removal of the glycans. This is a remarkably slight effect of a massive covalent modification, which reduces the molecular weight by ~20%, although the glycans as such do not define the structure or fold of the protein itself. Moreover, the fact that the catalytic activity of phytase found here and elsewhere (*16*, *49*) remains practically unchanged following deglycosylation suggests that the overall fold of the peptide is unchanged by the modification. This consistency of structure and stability makes the Phy/dgPhy system ideally suited for studies of the roles of the glycans. The nonequilibrium step of eq 7, on the other hand, is strongly suppressed by the glycans. Our results suggest that this stabilization of the monomeric denatured protein relies on steric hindrance of favorable electrostatic interactions in the aggregating protein introduced by the bulky glycans. This hindrance could be brought about by several mechanisms. The glycans may limit the structural flexibility of the denatured Phy molecule and thus hinder optimal interactions in the aggregate. Alternatively, the glycans might obstruct packing in the aggregates by hampering the formation of secondary structure elements in the aggregates.

The suggestion of a mechanism based on steric hindrance is supported by investigations of glycan dynamics. Several NMR studies, for example, have shown restrictions of the rotation around certain bonds and concluded that the glycan conformation is often controlled by steric limitations (*58*−*61*). Furthermore, it has been suggested that the saccharide groups show rather infrequent hydrogen bonding with the peptide in crystallized glycoproteins (*62*) and that the glycans of Phy are fully accessible to water in the native state (*16*). This view of a rather rigid and protruding structure of glycans is in accord with the suggestion that they hinder the irreversible aggregation of glycoproteins by disrupting the packing in the aggregate.

REFERENCES

1. Trombetta, E. S. (2003) The contribution of N-glycans and their Processing in the Endoplasmic Reticulum to Glycoprotein Biosynthesis, *Glycobiology 13*, 77−91.
2. Helenius, A. (1994) How N-linked Oligosaccharides Affect Glycoprotein Folding in the Endoplasmic Reticulum, *Mol. Biol. Cell 5*, 253−265.
3. Paulson, J. C. (1989) Glycoprotiens: What are the sugar chains for? *Trends Biochem. Sci. 14*, 272−276.
4. Tams, J. W., and Welinder, K. G. (1998) Glycosylation and thermodynamic versus kinetic stability of horseradish peroxidase, *FEBS Lett. 421*, 234−236.
5. Tams, J. W., and Welinder, K. G. (2001) Kinetic stability of designed glycosylation mutants of *Coprinus cinereus* peroxidase, *Biochem. Biophys. Res. Commun. 286*, 701−706.
6. Kwon, K. S., and Yu, M. H. (1997) Effect of glycosylation on the stability of α1-antitrypsin toward urea denaturation and thermal deactivation, *Biochim. Biophys. Acta 1335*, 265−272.

7. Price, N. J., Pinheiro, C., Soares, C. M., Ashford, D. A., Ricardo, C. P., and Jackson, P. A. (2003) A biochemical and molecular characterization of LEP1, an extensin peroxidase from lupin, *J. Biol. Chem. 278*, 41389−41399.
8. Cruz, M. A., Handin, R. I., and Wise, R. J. (1993) The interaction of the von Willebrand factor-A1 domain with platelet glycoprotein Ib/IX. The role of glycosylation and disulfide bonding in a monomeric recombinant A1 domain protein, *J. Biol. Chem. 268*, 21238−21245.
9. Maruyama, N., Katsube, T., Wada, Y., Oh, M. H., Barba De La Rosa, A. P., Okuda, E., Nakagawa, S., and Utsumi, S. (1998) The roles of the N-linked glycans and extension regions of soybean β-conglycinin in folding, assembly and structural features, *Eur. J. Biochem. 258*, 854−862.
10. Kern, G., Schulke, N., Schmid, F. X., and Jaenicke, R. (1992) Stability, quaternary structure, and folding of internal, external, and core-glycosylated invertase from yeast, *Protein Sci. 1*, 120−131.
11. Schulke, N., and Schmid, F. X. (1988) Effect of glycosylation on the mechanism of renaturation of invertase from yeast, *J. Biol. Chem. 263*, 8832−8837.
12. Ioannou, Y. A., Zeidner, K. M., Grace, M. E., and Desnick, R. J. (1998) Human α-galactosidase A: Glycosylation site 3 is essential for enzyme solubility, *Biochem. J. 332*, 789−797.
13. Haki, G. D., and Rakshit, S. K. (2003) Developments in Industrially Important Thermostable Enzymes: A review, *Bioresour. Technol. 89*, 17−34.
14. Kendrick, B. S., Carpenter, J. F., Cleland, J. L., and Randolph, T. W. (1998) A Transient Expansion of the Native State Precedes Aggregation of Recombinant Human Interferon-γ, *Proc. Natl. Acad. Sci. U.S.A. 94*, 14142−14146.
15. Eijsink, V. G., Bjork, A., Gaseidnes, S., Sirevag, R., Synstad, B., van den Burg, B., and Vriend, G. (2004) Rational Engineering of Enzyme Stability, *J. Biotechnol. 113*, 105−120.
16. Bagger, H. L., Fuglsang, C. C., and Westh, P. (2003) Preferential binding of two compatible solutes to the glycan moieties of *Peniophora lycii* phytase, *Biochemistry 42*, 10295−10300.
17. Lei, X. G., and Stahl, C. H. (2001) Biotechnological development of effective phytases for mineral nutrition and environmental protection, *Appl. Microbiol. Biotechnol. 57*, 474−481.
18. Lassen, S. F., Breinholt, J., Ostergaard, P. R., Brugger, R., Bischoff, A., Wyss, M., and Fuglsang, C. C. (2001) Expression, gene cloning, and characterization of five novel phytases from four basidiomycete fungi: *Peniophora lycii*, *Agrocybe pediades*, a *Ceriporia* sp., and *Trametes pubescens*, *Appl. Environ. Microbiol. 67*, 4701−4707.
19. Trimble, R. B., and Tarentino, A. L. (1991) Identification of distinct endoglycosidase (endo) activities in *Flavobacterium meningosepticum*: endo F1, endo F2, and endo F3. Endo F1 and endo H hydrolyze only high mannose and hybrid glycans, *J. Biol. Chem. 266*, 1646−1651.
20. Zimm, B. H. (1948) The scattering of light and the radial distribution function of high polymer solutions, *J. Chem. Phys. 16*, 1093−1099.
21. Bloomfield, V. A. (2000) Static and dynamic light scattering from aggregating particles, *Biopolymers 54*, 168−172.
22. Webb, J. N., Webb, S. D., Cleland, J. L., Carpenter, J. F., and Randolph, T. W. (2001) Partial molar volume, surface area, and hydration changes for equilibrium unfolding and formation of aggregation transition state: High-pressure and cosolute studies on recombinant human IFN-γ, *Proc. Natl. Acad. Sci. U.S.A. 98*, 7259−7264.
23. Chang, S. T., Tobler, S. A., and Fernandez, E. J. (2001) Unfolding and conformational distributions during protein precipitation, *Biotechnol. Prog. 17*, 583−585.
24. Rochet, J. C., and Lansbury, P. T., Jr. (2000) Amyloid fibrillogenesis: Themes and variations, *Curr. Opin. Struct. Biol. 10*, 60−68.
25. Kim, Y. S., Cape, S. P., Chi, E., Raffen, R., Wilkins-Stevens, P., Stevens, F. J., Manning, M. C., Randolph, T. W., Solomon, A., and Carpenter, J. F. (2001) Counteracting effects of renal solutes on amyloid fibril formation by immunoglobulin light chains, *J. Biol. Chem. 276*, 1626−1633.
26. Chi, E. Y., Krishnan, S., Kendrick, B. S., Chang, B. S., Carpenter, J. F., and Randolph, T. W. (2003) Roles of conformational stability and colloidal stability in the aggregation of recombinant human granulocyte colony-stimulating factor, *Protein Sci. 12*, 903−913.
27. Lumry, R., and Eyring, H. (1954) Conformation changes of proteins, *J. Phys. Chem. 58*, 110−120.
28. Sanchez-Ruiz, J. M., Lopez-Lacomba, J. L., Cortijo, M., and Mateo, P. L. (1988) Differential scanning calorimetry of the irreversible thermal denaturation of thermolysin, *Biochemistry 27*, 1648−1652.
29. Kreimer, D. I., Shnyrov, V. L., Villa, R. E., Silman, I., and Weiner, L. (1995) Irreversible thermal denaturation of *Torpedo californica* acetylcholinesterase, *Protein Sci. 4*, 2349−2357.
30. Lyubarev, A. E., Kurganov, B. I., Orlov, V. N., and Zhou, H. M. (1999) Two-state irreversible thermal denaturation of muscle creatine kinase, *Biophys. Chem. 79*, 199−204.
31. Creveld, L. D., Meijberg, W., Berendsen, H. J. C., and Pepermans, H. A. M. (2001) DSC studies of *Fusarium solani pisi* cutinase: Consequences for stability in the presence of surfactants, *Biophys. Chem. 92*, 65−75.
32. Weijers, M., Barneveld, P. A., Cohen Stuart, M. A., and Visschers, R. W. (2003) Heat-induced denaturation and aggregation of ovalbumin at neutral pH described by irreversible first-order kinetics, *Protein Sci. 12*, 2693−2703.
33. Gouda, M. D., Singh, S. A., Rao, A. G., Thakur, M. S., and Karanth, N. G. (2003) Thermal inactivation of glucose oxidase. Mechanism and stabilization using additives, *J. Biol. Chem. 278*, 24324−24333.
34. Kurganov, B. I., Rafikova, E. R., and Dobrov, E. N. (2002) Kinetics of thermal aggregation of tobacco mosaic virus coat protein, *Biochemistry (Moscow) 67* (5), 525−533.
35. Kendrick, B. S., Cleland, J. L., Lam, X., Nguyen, T., Randolph, T. W., Manning, M. C., and Carpenter, J. F. (1998) Aggregation of recombinant human interferon γ: Kinetics and structural transitions, *J. Pharm. Sci. 87*, 1069−1076.
36. Kurganov, B. I. (2002) Kinetics of protein aggregation. Quantitative estimation of the chaperone-like activity in test-systems based on suppression of protein aggregation, *Biochemistry (Moscow) 67*, 409−422.
37. Wang, K., and Kurganov, B. I. (2003) Kinetics of heat- and acidification-induced aggregation of firefly luciferase, *Biophys. Chem. 106*, 97−109.
38. Finke, J. M., Gross, L. A., Ho, H. M., Sept, D., Zimm, B. H., and Jennings, P. A. (2000) Commitment to folded and aggregated states occurs late in interleukin-1β folding, *Biochemistry 39*, 15633−15642.
39. Duy, C., and Fitter, J. (2005) Thermostability of irreversible unfolding of α-amylases analyzed by unfolding kinetics, *J. Biol. Chem. 280*, 37360−37365.
40. Hinrichs, J., and Rademacher, B. (2004) High pressure thermal denaturation kinetics of whey proteins, *J. Dairy Res. 71*, 480−488.
41. Weijers, M., Barneveld, P. A., Stuart, M. A. C., and Visschers, R. W. (2003) Heat-induced denaturation and aggregation of ovalbumin at neutral pH described by irreversible first-order kinetics, *Protein Sci. 12*, 2693−2703.
42. LeBon, C., Nicolai, T., and Durand, D. (1999) Kinetics of aggregation and gelation of globular proteins after heat induced denaturation, *Macromolecules 32*, 6120−6127.
43. Nohara, D., Mizutani, A., and Sakai, T. (1999) Kinetic study on the thermal denaturation of hen egg-white lysozyme involving precipitation, *J. Biosci. Bioeng. 87*, 199−205.
44. Collins, K. D., and Washabaugh, M. W. (1985) The Hofmeister effect and the behaviour of water at interfaces, *Q. Rev. Biophys. 18*, 323−422.
45. Baldwin, R. L. (1996) How Hofmeister ion interactions affect protein stability, *Biophys. J. 71*, 2056−2063.
46. Militello, V., Casarino, C., Emanuele, A., Giostra, A., Pullara, F., and Leone, M. (2004) Aggregation kinetics of bovine serum albumin studied by FTIR spectroscopy and light scattering, *Biophys. Chem. 107*, 175−187.
47. Durbin, S. D., and Feher, G. (1996) Protein crystallization, *Annu. Rev. Phys. Chem. 47*, 171−204.
48. van Holde, K. E., Johnson, W. C., and Ho, P. S. (1998) *Principles of Physical Biochemistry*, Prentice Hall, Upper Saddle River, NJ.
49. Bagger, H. L., Fuglsang, C. C., and Westh, P. (2005) Hydration of a glycoprotein: Relative water affinity of peptide and glycan moieties, *Eur. Biophus. J.* (in press).
50. Tams, J. W., Vind, J., and Welinder, K. G. (1999) Adapting protein solubility by glycosylation. N-Glycosylation mutants of *Coprinus cinereus* peroxidase in salt and organic solutions, *Biochim. Biophys. Acta 1432*, 214−221.
51. Tams, J. W., and Welinder, K. G. (1995) Mild chemical deglycosylation of horseradish peroxidase yields a fully active, homogeneous enzyme, *Anal. Biochem. 228*, 48−55.

52. Mimura, Y., Church, S., Ghirlando, R., Ashton, P. R., Dong, S., Goodall, M., Lund, J., and Jefferis, R. (2000) The influence of glycosylation on the thermal stability and effector function expression of human IgG1-Fc: Properties of a series of truncated glycoforms, *Mol. Immunol. 37*, 697−706.
53. Wang, C., Eufemi, M., Turano, C., and Giartosio, A. (1996) Influence of the carbohydrate moiety on the stability of glycoproteins, *Biochemistry 35*, 7299−7307.
54. Srinivas, V. R., Singha, N. C., Schwarz, F. P., and Surolia, A. (1998) Differential scanning calorimetric studies of the glycoprotein, winged bean acidic lectin, isolated from the seeds of *Psophocarpus tetrogonolobus*, *FEBS Lett. 425*, 57−60.
55. van Zuylen, C. W., Kamerling, J. P., and Vliegenthart, J. F. (1997) Glycosylation beyond the Asn78-linked GlcNAc residue has a significant enhancing effect on the stability of the α subunit of human chorionic gonadotropin, *Biochem. Biophys. Res. Commun. 232*, 117−120.
56. Hashimoto, Y., Munemura, O., Masumoto, K., Ueda, T., and Imoto, T. (2001) Thermostability of Doubly Glycosylated Recombinant Lysosyme, *Biol. Pharm. Bull. 24*, 1102−1107.
57. Pfeil, W. (2002) The influence of glycosylation on the thermal stability of ribonuclease, *Thermochim. Acta 382*, 169−174.
58. Cumming, D. A., and Carver, J. P. (1987) Virtual and solution conformations of oligosaccharides, *Biochemistry 26*, 6664−6676.
59. Rutherford, T. J., Partridge, J., Weller, C. T., and Homans, S. W. (1993) Characterization of the extent of internal motions in oligosaccharides, *Biochemistry 32*, 12715−12724.
60. Lommerse, J. P., Kroon-Batenburg, L. M., Kamerling, J. P., and Vliegenthart, J. F. (1995) Conformational analysis of the xylose-containing N-glycan of pineapple stem bromelain as part of the intact glycoprotein, *Biochemistry 34*, 8196−8206.
61. Lommerse, J. P., van Rooijen, J. J., Kroon-Batenburg, L. M., Kamerling, J. P., and Vliegenthart, J. F. (2002) Conformational analysis of two xylose-containing N-glycans in aqueous solution by using ^{1}H NMR ROESY and NOESY spectroscopy in combination with MD simulations, *Carbohydr. Res. 337*, 2279−2299.
62. Imberty, A., and Perez, S. (1995) Stereochemistry of the N-glycosylation sites in glycoproteins, *Protein Eng. 8*, 699−709.

BI0522955